Thermoelectric properties of *n*-type $Bi_2(Te_{0.85}Se_{0.15})_3$ single crystals doped with CuBr and SbI_3

Ö. Ceyda Yelgel and G. P. Srivastava
School of Physics, University of Exeter, Stocker Road, Exeter EX4 4QL, United Kingdom
(Received 31 August 2011; revised manuscript received 16 March 2012; published 29 March 2012)

In this work we present a systematic investigation of the thermoelectric properties of semiconductor alloys. Electronic properties (Fermi energy, Seebeck coefficient, and electrical resistivity) are calculated in both extrinsic and intrinsic regimes using the nearly-free-electron approximation and the Fermi-Dirac statistics. The lattice thermal conductivity is computed by including anharmonic phonon interactions rigorously. The thermal conductivity contributions from donor electrons, and electron-hole pairs are also taken into account. We successfully explain the previously reported experimental measurements of the magnitude as well as temperature dependence of the electronic and thermal transport coefficients, as well as the thermoelectric figure of merit ZT for the $Bi_2(Te_{0.85}Se_{0.15})_3$ single crystal with 0.1 wt % CuBr and 0.2 wt % SbI_3 dopants. The frequency dependence of thermal conductivity is investigated in detail for a 0.2 wt % SbI_3-doped sample at several temperatures. Furthermore, the effect of alloying on the thermoelectric efficiency of $(Bi_2Te_3)_x(Bi_2Se_3)_{(1-x)}$ single crystals is explored.

DOI: 10.1103/PhysRevB.85.125207 PACS number(s): 72.20.Pa, 66.70.Df

I. INTRODUCTION

Thermoelectric (TE) devices are capable of directly converting temperature differences to electric voltage and vice versa. By transforming heat generated from industrial processes, solar radiation, automotive exhaust, or other sources to electricity, they work as a thermoelectric power generator. Conversely, to make cooling systems such as refrigerators or portable beverage coolers, they work as a thermoelectric cooler. Having no moving parts and being silent, extremely reliable, scalable, and environmentally friendly, thermoelectric devices provide a possible solution for present and future energy challenges.[1–4] To find the best thermoelectric material, it is required to investigate its thermoelectric efficiency, which is assessed in terms of the dimensionless figure of merit, ZT:

$$ZT = \frac{\sigma S^2}{\kappa} T, \tag{1}$$

where S, σ, and κ are the Seebeck coefficient, the electrical conductivity, and the thermal conductivity, respectively. There are limited choices for finding materials in nature that exhibit a high figure of merit (i.e., with $ZT > 1$). Previous research has concluded that doped semiconducting materials are among the most efficient TE materials.[5,6] In semiconductors heat is transferred by electrons (κ_{el}), phonons (κ_{ph}), and electron-hole pairs (bipolar contribution κ_{bp}), with phonon contribution being the most significant.

Increasing ZT in semiconductors by reducing phonon thermal conductivity can be done without decreasing electrical conductivity.[7] One route for reducing phonon conductivity is by making alloys. It has long been known that semiconductor alloys with high carrier concentration are among the best bulk thermoelectrics.[8] Two examples are the Bi_2Te_3-Bi_2Se_3 or Si-Ge alloys (two isostructural semiconductors), which with strong point defect scattering exhibit low phonon thermal conductivity and are the best commercially available thermoelectric materials.[8] Another possible route to improve ZT is by reducing the phonon thermal conductivity via fabrication of low-dimensional structures, such as quantum wells, wires, superlattices, or dots. Reduction in the lattice thermal conductivity in such structures is caused by phonon interface scattering, leading to significant improvement in ZT.[4,9–12] More recent examples of this approach are p-type Bi_2Te_3/Sb_2Te_3 superlattices, reported to be among the best thermoelectric materials with $ZT \sim 2.4$ at room temperature.[10]

In order to make a quantitative assessment of ZT for a given material, and prediction for other materials (such as alloys of two materials with different fractional contents), it is important to develop accurate theoretical models for the transport coefficients S, σ, κ_{el}, κ_{ph}, and κ_{bp}. A large number of publications have been devoted in this respect (see, e.g., Refs. 1, 6, 13, and references therein). However, most works do not explicitly discuss the cases of extrinsically doped and intrinsic (undoped) semiconductors and do not clearly account for the temperature variation of Fermi energy. Furthermore, to the best of our knowledge, all previous works have treated phonon transport (lattice thermal conductivity κ_{ph}) in an *ad hoc* manner, using simplified expressions for alloying and anharmonic phonon interactions, utilizing several adjustable parameters. Many approaches do not distinguish between phonon scattering due to point (i.e., isotopic) defects and phonon scattering due to alloying effect. Almost all previous works treat the effect of anharmonic phonon interaction in κ_{ph} using a combination of adjustable parameters and an interpolative scheme. For example, Vining[14] considered a single-phonon polarization branch and used the frequency and temperature dependence of the form $\omega^2 T$ for the umklapp three-phonon scattering rate and expressed the normal three-phonon scattering rate as a scaled version of the former. These frequency and temperature considerations are normally valid in the high-temperature range. The normal and umklapp relaxation processes are characterized by different frequency and temperature dependencies at low temperatures, and a constant ratio for their rates is an unvalidated consideration. As the role of κ_{ph} is regarded as much more important than the role of other transport coefficients in enhancing ZT for low-dimensional semiconductors,[4,9–12] it is very important to use a well-founded theory of κ_{ph} that includes anharmonic

phonon interactions without the need for many adjustable parameters.

In this work we follow the Hicks-Dresselhaus theory[15] for S, σ, and κ_{el}, Srivastava's detailed theory[16] of lattice thermal conductivity κ_{ph}, and Price's theory[17] of κ_{bp} to study the temperature dependencies of Fermi energy, Seebeck coefficient, electrical conductivity, and all contributions of thermal conductivity of n-type 85% Bi_2Te_3/15% Bi_2Se_3 single crystals doped with 0.1 wt % CuBr and 0.2 wt % SbI_3 samples. The temperature variation of the Fermi energy,[18] covering the extrinsic and intrinsic conditions, is taken into account. Our calculated results for the thermoelectric transport coefficients are compared with the experimental values obtained by Hyun *et al.*[19] A discussion is provided to explain the difference in ZT for the two samples.

II. THEORETICAL CONSIDERATIONS

A. Electronic properties

1. Fermi energy

The electronic transport coefficients S, σ, and κ_{el} required for an evaluation of the thermoelectric figure of merit, ZT, for a semiconductor depend on the temperature dependence of the Fermi energy E_F. The temperature variation of the Fermi energy in an n-doped semiconductor is given by[18]

$$E_F^{ext} = \frac{1}{2}(E_c + E_d) + \frac{k_B T}{2}\ln\frac{N_d}{2U_c} - k_B T \sinh^{-1} \times \left[\sqrt{\frac{U_c}{8N_d}}\exp\left(\frac{-\Delta E_i}{2k_B T}\right)\right], \quad (2)$$

where E_c is the conduction band edge, E_d is the donor energy level, N_d is the concentration of donor impurity atoms, $\Delta E_i = E_c - E_d$ is the donor ionization energy, and $U_c = 2[(m_n^* k_B T)/(2\pi\hbar^2)]^{3/2}$, with m_n^* as the electron mass, k_B the Boltzmann constant, and $\hbar$ the reduced Planck constant.

At absolute zero temperature the Fermi level lies halfway between the donor level and the conduction band edge. As temperature increases, it first goes up slightly (while remaining below the conduction band edge) and then decreases below the donor level toward the center of the band gap of the semiconductor. Beyond a sufficiently high temperature, donors at the E_d level are completely ionized and the material becomes an intrinsic semiconductor, and consequently the temperature variation of the Fermi level is given by[18]

$$E_F^{int} = \frac{E_v + E_c}{2} + \frac{3}{4}k_B T \ln\left(\frac{m_p^*}{m_n^*}\right), \quad (3)$$

where E_v is the valence band edge and m_p^* is the hole effective mass. With the conduction band edge set to zero ($E_c = 0$), Eq. (3) can be written in terms of the energy gap E_g. We have attempted a simple expression[20] of the form $E_g(T) = E_g(0) - \alpha T$, with α considered as an adjustable parameter, to obtain the best fit for the temperature variation of E_F, S, and σ in the intrinsic regime. With this choice, the Fermi energy in the intrinsic regime can be expressed as

$$E_F^{int} = -\frac{1}{2}[E_g(0) - \alpha T] + \frac{3}{4}k_B T \ln\left(\frac{m_p^*}{m_n^*}\right). \quad (4)$$

2. Seebeck coefficient

Within a single-band nearly-free-electron consideration, the Seebeck coefficient (S) and the electrical conductivity (σ) can be defined in terms of Fermi energy by using Fermi-Dirac statistics. Accordingly, the Seebeck coefficient can be written as[7,20]

$$S = \pm\frac{k_B}{e}(\delta - \zeta^*), \quad (5)$$

where the minus sign is for n-type materials, the plus sign is for p-type materials, e is the electronic charge, $\zeta^* = E_f/k_B T$ is the reduced chemical potential, and δ is given by[7,20]

$$\delta = \frac{\left(r + \frac{5}{2}\right)F_{r+\frac{3}{2}}(\zeta^*)}{\left(r + \frac{3}{2}\right)F_{r+\frac{1}{2}}(\zeta^*)}, \quad (6)$$

with r as a scattering parameter which we take as 0.1 from the work of Hyun *et al.*[19] and F_r as the Fermi integral written as[15]

$$F_r = \int_0^\infty \frac{x^i dx}{e^{(x-\zeta^*)} + 1}. \quad (7)$$

3. Electrical conductivity

Similarly, within the single-band nearly-free-electron model, the electrical conductivity in the extrinsic regime of a semiconductor can be expressed as[20,21]

$$\sigma = ne\mu_c = n\frac{e^2}{m_c^*}\langle\tau\rangle, \quad (8)$$

where μ_c is the conductivity mobility, m_c^* is the conductivity effective mass (taken as m_n^*), $\langle\tau\rangle$ is an average relaxation time for carriers, and n is the carrier concentration defined as[21,22]

$$n = \int_0^\infty g(E) f_0(E) dE = \frac{4}{\sqrt{\pi}}\left(\frac{m_D^* k_B T}{2\pi\hbar^2}\right)^{3/2} F_{1/2}(\zeta^*), \quad (9)$$

with $g(E)$ representing the density of states for a nearly-free-electron gas, $f_0(E)$ the Fermi-Dirac distribution function, and m_D^* the density-of-states effective mass.

In n-type doped single crystals electrons mostly interact with the long-wavelength phonons (which have low energy). The scattering rate for the dominant scattering involving acoustic phonons can be written as[7,23]

$$\tau_{ac}^{-1}(E,T) = \frac{\sqrt{2}}{\pi}\frac{E_D^2 m_D^{*3/2} k_B T}{\hbar^4 \rho c_L^2}\sqrt{E}, \quad (10)$$

where c_L is the velocity of longitudinal phonons, ρ is the mass density, and E_D is the deformation potential. Using this, we express the average relaxation time as[21]

$$\langle\tau\rangle = \frac{\int \tau(W) W^{3/2}\exp(-W)\mathrm{d}W}{\int W^{3/2}\exp(-W)\mathrm{d}W} = \frac{4}{3}\sqrt{\frac{\pi}{2}}\frac{\hbar^4\rho c_L^2}{E_D^2 m_D^{*3/2}(k_B T)^{3/2}}, \quad (11)$$

with $W = E/k_B T$.

Thus, from Eqs. (8), (9), and (11) the electrical conductivity in the extrinsic regime can be expressed as

$$\sigma = \frac{4}{3\pi\sqrt{\pi}} \frac{e^2}{m_c^*} \frac{\hbar \rho c_L^2}{E_D^2} F_{1/2} \tag{12}$$

when only acoustic phonon scattering is considered.

In the intrinsic regime, electrical conductivity is expressed as[18,24]

$$\sigma_{\text{intrinsic}} = e n_i (\mu_n + \mu_p) = A' e^{-E_g/2k_b T}, \tag{13}$$

where n_i is the equilibrium carrier density, μ_n, μ_p are the electron and hole mobilities, respectively, and A' is a parameter that does not strongly depend on temperature.

B. Thermal properties

The total thermal conductivity (κ) in semiconductors has three contributions: electronic (κ_{el}), lattice (i.e., from phonons, κ_{ph}), and bipolar (i.e., from electron-hole pairs, κ_{bp}).

1. Electronic thermal conductivity

The electronic part of the thermal conductivity is given by the Wiedemann-Franz law[20]

$$\kappa_{\text{el}} = \sigma \mathcal{L} T = \left(\frac{k_B}{e}\right)^2 \sigma T \mathcal{L}_0, \tag{14}$$

where $\mathcal{L}$ is the Lorenz number and $\mathcal{L}_0$ can be written as[7,19,20]

$$\mathcal{L}_0 = \frac{\left(r+\frac{7}{2}\right) F_{r+\frac{5}{2}}(\zeta^*)}{\left(r+\frac{3}{2}\right) F_{r+\frac{1}{2}}(\zeta^*)} - \left[\frac{\left(r+\frac{5}{2}\right) F_{r+\frac{3}{2}}(\zeta^*)}{\left(r+\frac{3}{2}\right) F_{r+\frac{1}{2}}(\zeta^*)}\right]^2. \tag{15}$$

2. Bipolar thermal conductivity

The bipolar (electron-hole pair) thermal conductivity (κ_{bp}) becomes a dominant contribution above 300 K in small-band-gap semiconductors such as Bi_2Te_3, PbTe, and PbSe. This contribution can be expressed as[25]

$$\kappa_{\text{bp}} = \frac{b}{(1+b)^2} \left[\frac{E_g}{k_B T} + 4\right]^2 \left[\frac{k_B}{e}\right]^2 \sigma_{\text{intrinsic}} T, \tag{16}$$

where b is the ratio of electron mobility to hole mobility. With Eqs. (13) and (16) we express the bipolar part of the thermal conductivity as

$$\kappa_{\text{bp}} = F_{\text{bp}} T^p \exp(-E_g/2k_B T), \tag{17}$$

and we regard F_{bp} and p as adjustable parameters, changing with doping type.

3. Lattice thermal conductivity

Within the single-mode relaxation time approximation, and adopting Debye's isotropic continuum scheme, the lattice thermal conductivity can be expressed as[16]

$$\kappa_{\text{ph}} = \frac{\hbar^2 q_D^5}{6\pi^2 k_B T^2} \sum_s c_s^4 \int_0^1 dx x^4 \tau \bar{n}(\bar{n}+1), \tag{18}$$

where q_D is the Debye radius, $x = q/q_D$ is a reduced wave number, s is the phonon polarization index (i.e., indicating longitudinal and transverse branches), $\bar{n}$ is the Bose-Einstein distribution function, and c_s is the velocity of phonons in polarization s. The phonon relaxation time τ in Eq. (18) is governed by different scattering mechanisms. Within Matthiessen's rule we can express $\tau^{-1} = \sum_i \tau_i^{-1}$, where τ_i^{-1} represents contributions from the ith scattering mechanism. The contributions from phonon scattering mechanisms relevant to the present study are listed below.

Phonon scattering from sample boundaries is given by[16,23]

$$\tau_{qs}^{-1}(bs) = \frac{c_s}{L}, \tag{19}$$

where L is the mean free path defined from the crystal size. In n-type alloy samples, phonons can suffer scattering from two types of mass defects: isotopic point defects and mass difference due to alloying. The phonon scattering rate from both types of mass defects can be expressed using the formula[16]

$$\tau_{qs}^{-1}(\text{md}) = \frac{\Gamma_{\text{md}} \Omega}{4\pi \bar{c}^3} \omega^4(qs), \tag{20}$$

where Ω is the volume of a unit cell, $\bar{c}$ is the average phonon speed, $\omega = cq$, and Γ_{md} is the mass-defect parameter. For a single-species crystal, the isotopic mass-defect parameter takes the form[26]

$$\Gamma_{\text{isotopes}} = \sum_i f_i \left(\frac{\Delta M_i}{\bar{M}}\right)^2, \tag{21}$$

where f_i is the percentage of the ith isotope present in the crystal and $\Delta M_i = M_i - \bar{M}$, where M is the average atomic mass. For a composite material, such as an alloy, with molecular formula $A_x B_y C_z \cdots$ the mass-defect parameter is given by[26]

$$\begin{aligned}\Gamma_{\text{alloy}}(A_x B_y C_z \cdots) &= \frac{x}{(x+y+z+\cdots)} \left(\frac{M_A}{\bar{M}}\right)^2 \Gamma(A) \\ &+ \frac{x}{(x+y+z+\cdots)} \left(\frac{M_B}{\bar{M}}\right)^2 \Gamma(B) \\ &+ \frac{x}{(x+y+z+\cdots)} \left(\frac{M_C}{\bar{M}}\right)^2 \Gamma(C) + \cdots,\end{aligned} \tag{22}$$

where $\Gamma(A) = \sum_i f_i (\frac{\Delta M_i(A)}{\bar{M}_A})^2$ represents the defect parameter for atomic species A, and the average atomic mass is expressed as $\bar{M} = (xM_A + yM_B + zM_C + \cdots)/(x+y+z+\cdots)$.

For moderately n-doped semiconductors, the scattering rate of longitudinal phonons of frequency ω by donor electrons of effective mass m^* (taken as m_n^*) and concentration n (taken as N_d) can be expressed as[27]

$$\tau_{ql}^{-1}(\text{ep}) = \frac{n E_D^2 \omega}{\rho c_L^2 k_B T} \sqrt{\frac{\pi m^* c_L^2}{2k_B T}} \exp\left(\frac{-m^* c_L^2}{2k_B T}\right). \tag{23}$$

For the anharmonic phonon interaction we restrict ourselves to only three-phonon scattering events. Following Srivastava's scheme, we express the anharmonic phonon scattering rate as[16]

$$\tau_{qs}^{-1}(3\text{ph}) = \frac{\hbar q_D^5 \gamma^2}{4\pi\rho\bar{c}^2} \sum_{s's''\varepsilon} \left[\left\{ \int dx' x'^2 x''_+ [1 - \varepsilon + \varepsilon(Cx + Dx')] \times \frac{\bar{n}_{q's'}(\bar{n}''_+ + 1)}{(\bar{n}_{qs} + 1)} + \frac{1}{2} \int dx' x'^2 x''_- [1 - \varepsilon + \varepsilon(C - Dx')] + \frac{\bar{n}_{q's'}\bar{n}''_-}{\bar{n}_{qs}} \right\} \right], \quad (24)$$

where γ is the Grüneisen constant, $x' = q'/q_D$, $x_\pm = Cx \pm Dx'$ and $\bar{n}''_\pm = \bar{n}(x''_\pm)$, $C = c_s/c_{s''}$, $D = c_{s'}/c_{s''}$, $\varepsilon = 1$ for momentum-conserving normal processes (N processes), and $\varepsilon = -1$ for non-momentum-conserving umklapp processes (U processes). The first and second terms in the above equation represent class 1 events $\boldsymbol{q}s + \boldsymbol{q}'s' \rightarrow \boldsymbol{q}''s''$ and class 2 events $\boldsymbol{q}s \rightarrow \boldsymbol{q}'s' + \boldsymbol{q}''s''$, respectively. In the present work we express three-phonon interactions in terms of the parameter defined as $F_{3\text{ph}} = (\frac{\gamma}{\bar{c}})^2$. The integration limits on the variables x and x', derived from a detailed consideration of the energy and momentum conservation requirements, have been given as follows.[16]

Class 1 events:

$$\begin{aligned} &0 \leqslant x \leqslant 1 \\ &\text{N processes: } 0, \frac{(1-C)x}{(1+D)} \leqslant x' \leqslant \frac{(1+C)x}{(1-D)}, \frac{(1-Cx)}{D}, 1 \\ &\text{U processes: } 0, \frac{(2-(1+C)x)}{(1+D)} \leqslant x' \leqslant \frac{(1-Cx)}{D}, 1 \end{aligned} \quad (25)$$

Class 2 events:

$$\begin{aligned} &\text{N processes: } (0 \leqslant x \leqslant 1) \\ &0, \frac{(C-1)x}{(D+1)}, \frac{(Cx-1)}{D} \leqslant x' \leqslant \frac{(C+1)x}{(D+1)}, \frac{(C-1)x}{D-1}, 1 \\ &\text{U processes: } \left(\frac{2}{1+C} \leqslant x \leqslant 1 \right) \\ &0, \frac{(2-(1+C)x)}{(1-D)}, \frac{Cx-1}{D}, \frac{(C+1)x-2}{D+1} \leqslant x' \leqslant \frac{(C+1)x-2}{D-1}, 1. \end{aligned} \quad (26)$$

III. RESULTS OF CALCULATIONS AND DISCUSSION

To investigate the effect of doping and dopant type on ZT, results for $Bi_2(Te_{0.85}Se_{0.15})_3$ single crystals have been compared with 0.1 wt % CuBr and 0.2 wt % SbI_3 dopants. Relevant parameters used in our work are compiled in Table I. All integrals were evaluated numerically by employing Simpson's rule.

A. Electronic properties

1. Fermi energy

The theoretical calculation of Fermi energy–temperature curves for 0.1 wt % CuBr-doped and 0.2 wt % SbI_3-doped $Bi_2(Te_{0.85}Se_{0.15})_3$ single crystals are presented in Fig. 1. For comparison, we have also shown the Fermi energy values extracted by Hyun *et al.*[19] from their experimental measurements of the Seebeck coefficient. Based upon an analysis of the Seebeck coefficient and electrical resistivity, Hyun *et al.* find these two samples to exhibit the extrinsic behavior for the entire temperature range studied here. However, using the parameters listed in Table I, and as seen in Fig. 1, we find that the extrinsic regime ceases at around 500 K and 450 K for the CuBr- and SbI_3-doped samples, respectively. The inset in Fig. 1 shows the temperature variation of E_F by considering both samples as extrinsic.

In the extrinsic regime following Eq. (2), below 450 K for the SbI_3-doped sample and below 500 K for the CuBr-doped sample, the Fermi energy gently increases with temperature. At a given temperature, the Fermi energy is higher for the CuBr-doped sample than for the SbI_3-doped sample. This is because CuBr is a more efficient dopant and, despite a lower doping level, provides a higher concentration (N_d) of halogen donor atoms. For both samples, the weak temperature variation of E_F in the extrinsic regime is due to the opposite signs of terms 2 and 3 in Eq. (2).

In the intrinsic regime, following Eq. (4), E_F rises faster with temperature. We find that the parameter α, determining the temperature variation of the band gap E_g, is the decisive factor to match theory with experimentally deduced results. The difference in the extrinsic-intrinsic turnover temperatures for the two samples is due to the joint effect of N_d in the extrinsic regime and the E_g-T variation in intrinsic regime.

2. Seebeck coefficient

Our theoretical results for the Seebeck coefficient, shown in Fig. 2, are in reasonably good agreement with the experimentally measured values in the work of Hyun *et al.*[19] We

TABLE I. Constants and parameters used in the calculations of thermoelectric properties of a $Bi_2(Te_{0.85}Se_{0.15})_3$ single crystal doped with 0.1 wt % CuBr and 0.2 wt %SbI_3.

	85% Bi_2Te_3/15% Bi_2Se_3 Single Crystal	
Property/Parameter	0.1 wt % CuBr doped	0.2 wt % SbI_3 doped
$E_g(0)$ (eV)	0.21	0.21
E_d (eV)	−0.09	−0.09
α (eV/K)	0.0007	0.0008
N_d (m^{-3})	1.32×10^{25}	8.0×10^{24}
m_n^*/m_e [a]	0.056	0.056
m_p^*/m_e [a]	0.065	0.065
ρ (kg/m^3) [b]	7.7×10^3	7.7×10^3
c_L (m/s) [c]	4.76×10^3	4.76×10^3
c_T (m/s) [c]	2.325×10^3	2.325×10^3
a_{lat} (Å) [d]	4.346	4.346
E_D (eV)	32	32
ς	−0.3	−0.5
A	10.87 $K^{0.3}$	25 $K^{0.5}$
A' (Ω^{-1} m^{-1})	3.03×10^8	1.35×10^8
B (Ω m K^{-1})	1.6×10^{-8}	2.1×10^{-8}
B' (Ω) m $K^{-1/2}$)	7.0×10^{-8}	1.0×10^{-9}
p	1.0	1.0
F_{bp} (W/m K)	3.4×10^{-4}	2.4×10^{-4}
q_D ($Å^{-1}$)	0.7113	0.7113
L (mm)	5.0	5.0
Ω ($Å^3$)	164.94	164.94
Γ_{isotopes}	0.000112	0.00561
Γ_{alloy}	0.00447	0.00447
F_{3ph} (s^2/m^2)	0.2×10^{-5} (low temp.) 0.4×10^{-5}(high temp.)	0.2×10^{-5} (low temp.) 0.4×10^{-5} (high temp.)

[a]Reference 19.
[b]Reference 28.
[c]Reference 29.
[d]Reference 30.

expect the temperature variation of the Seebeck coefficient of the CuBr- and SbI_3-doped $Bi_2(Te_{0.85}Se_{0.15})_3$ single crystals to directly reflect the extrinsic-intrinsic turnover obtained for the corresponding E_F. This is indeed what is found, as shown in Fig. 2.

In the temperature region 100–450 K (viz., the extrinsic regime), the Seebeck coefficient depends on the Fermi energy directly [the second term in Eq. (5)] and via the Fermi integrals $F_{1/2}$ and $F_{3/2}$ [the first term in Eq. (5)]. Throughout this temperature range an asymptotic expansion of the Fermi integrals can be made.[31] As $\zeta^* > 1$, using the appropriate asymptotic expansion it can be shown that δ, the first term in Eq. (5), also varies linearly with the Fermi energy. Two points can be made from this simple analysis. First, the temperature variation of S seen in Fig. 2, thus, is nearly similar to that of the Fermi energy. Second, following the variation of E_F, the difference in S increases with temperature.

In accordance with the temperature variation of the Fermi energy, in the intrinsic regime the temperature variation of the Seebeck coefficient is much sharper for the SbI_3-doped sample. While the values of the Seebeck coefficient are similar for the two samples up to 450 K, results for the SbI_3-doped sample become progressively lower as temperature increases inside the intrinsic regime. At 600 K, the computed value for the SbI_3-doped sample is 12.4% lower than that for the CuBr-doped sample.

The inset in Fig. 2 shows the Seebeck coefficient results by treating the samples to exhibit the extrinsic behavior throughout the temperature range. It is clear that while the CuBr-doped sample may reasonably well be treated as being extrinsic, the SbI_3-doped sample must be treated as intrinsic above 450 K.

3. *Electrical resistivity*

The electrical resistivity results of CuBr- and SbI_3-doped alloys are shown in Fig. 3 with their reported experimental results by Hyun *et al.*[19]

To calculate the electrical resistivity in the extrinsic regime a number of different scattering mechanisms, arising from phonons (acoustic and optical phonon scatterings) and imperfections (neutral impurities, ionized impurities, and alloying effects) and carrier-carrier scatterings, need to be considered.[22] For our samples, the acoustic phonon scattering was found the most dominant scattering mechanism in the 100–600 K temperature range. Although the acoustic phonon scattering is taken as the main effective mechanism to express the electrical conductivity as in Eq. (12), the effect of other scattering mechanisms alters the magnitude as well as the

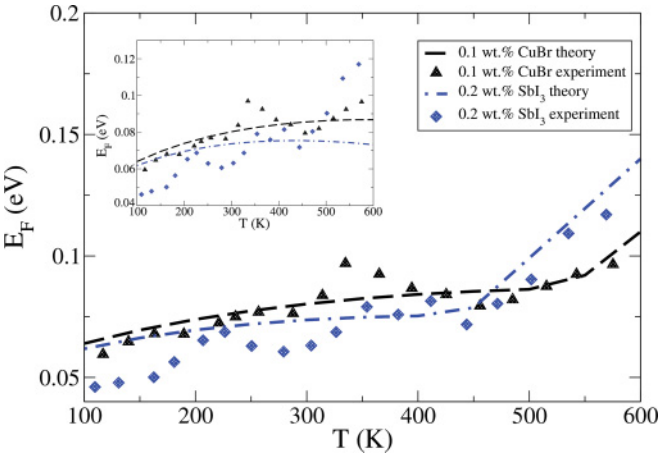

FIG. 1. (Color online) Temperature variation of Fermi energy for $Bi_2(Te_{0.85}Se_{0.15})_3$ single crystal doped with 0.1 wt % CuBr (dashed curve) and 0.2 wt % SbI_3 (dash-dotted curve). The symbols represent the results obtained from experimental measurements of the Seebeck coefficient by Hyun *et al.*[19] The inset shows the results of treating the samples as extrinsically doped throughout the entire temperature range. The bottom of the conduction band is taken as the zero along the energy axis (i.e., $E_c = 0$).

temperature dependence. Indeed, as noted before,[18] usually experimental electrical conductivity results are at variance with the prediction of Eq. (12), and it becomes necessary to scale both the magnitude and the temperature dependence of σ. We therefore express $\sigma_{\text{extrinsic}}$ in the following modified form:

$$\sigma_{\text{extrinsic}} = \sigma A T^{\varsigma}, \tag{27}$$

where A and ς are adjustable parameters.

In the temperature region 100–450 K (viz., the extrinsic regime), the electrical conductivity depends on the Fermi energy via the Fermi integral $F_{1/2}$. In this temperature range $\zeta^* > 1$, and using the appropriate asymptotic expansion[31] it can be noted that the Fermi integral $F_{1/2}$ is proportional to

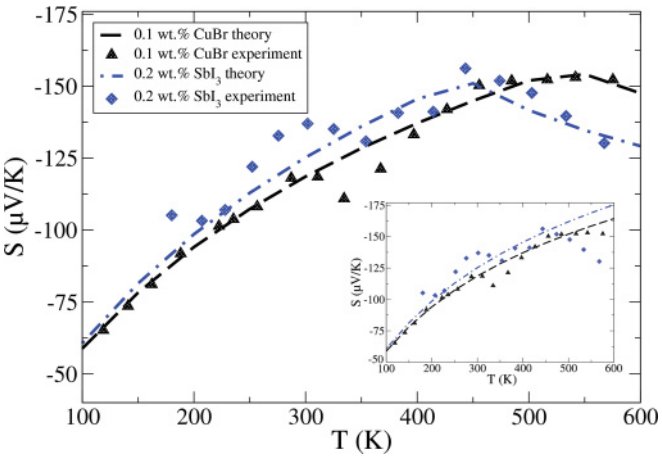

FIG. 2. (Color online) Temperature variation of Seebeck coefficient for $Bi_2(Te_{0.85}Se_{0.15})_3$ single crystal doped with 0.1 wt % CuBr (dashed curve) and 0.2 wt % SbI_3 (dash-dotted curve). The symbols represent the experimental results from Ref. 19. The inset shows the results of treating the samples as extrinsically doped throughout the entire temperature range.

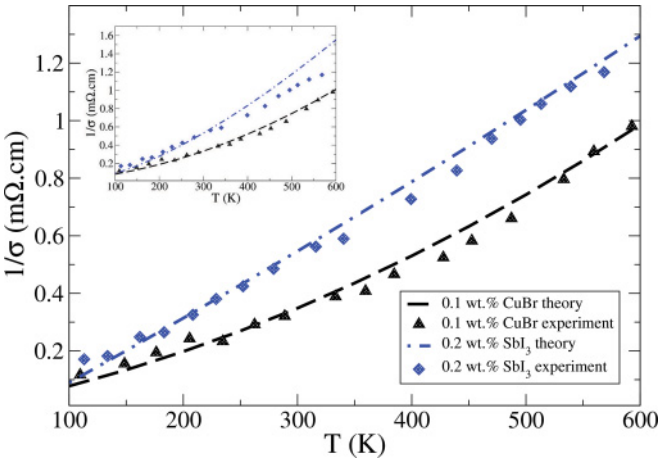

FIG. 3. (Color online) Temperature variation of electrical resistivity for $Bi_2(Te_{0.85}Se_{0.15})_3$ single crystal doped with 0.1 wt % CuBr (dashed curve) and 0.2 wt % SbI_3 (dash-dotted curve). The symbols represent the experimental results from Ref. 19. The inset shows the results of treating the samples as extrinsically doped throughout the entire temperature range.

$\zeta^{*3/2}$. Thus, at a given temperature, the higher Fermi energy for the CuBr-doped sample ensures that its resistivity is lower than that of the SbI_3-doped sample. In the intrinsic regime, the higher resistivity of the SbI_3-doped sample is achieved by the choice of the parameters A' and ς as presented in Table I.

In the intrinsic regime, the temperature dependence of the mobility usually cancels with the temperature dependence of the equilibrium carrier density. So, with a suitable choice of A' the electrical conductivity in the intrinsic regime is defined as in Eq. (13). In order to fully reproduce the experimental results in the intrinsic regime, we found it useful to add the free carrier–phonon scattering contribution. At these temperatures such scattering can be treated using metal physics, leading to $\rho_{\text{intrinsic}} = 1/\sigma_{\text{intrinsic}} + BT$.[32] The fitted value of the parameter B is listed in Table I.

We also managed to reproduce the results for the CuBr-doped sample beyond 500 K by treating it as extrinsic only and adding a contribution from carrier-optical phonon scattering. Optical phonons can be expected to be populated at these high temperatures.[22] Such a scattering rate can be expressed as $\rho_{(\text{full-extrinsic})} = 1/\sigma_{\text{extrinsic}} + B'\sqrt{T}$. The parameter B' is listed in Table I. Such an attempt, however, did not prove successful for the SbI_3-doped sample. The attempted results are shown in the inset of Fig. 3.

B. Thermal properties

1. *Electronic thermal conductivity*

The theoretical calculation of the electronic thermal conductivities of both CuBr- and SbI_3-doped samples are shown in Fig. 4. In accordance with the Wiedemann-Franz law, due to its lower resistivity, the CuBr-doped sample has bigger κ_{el} than the SbI_3-doped sample.

The electronic thermal conductivities of both samples decrease with temperature and the difference between κ_{el} results becomes progressively smaller as temperature increases. Our work suggests that the values of κ_{el} are 3.0 $\text{Wm}^{-1}\text{K}^{-1}$ at 100 K

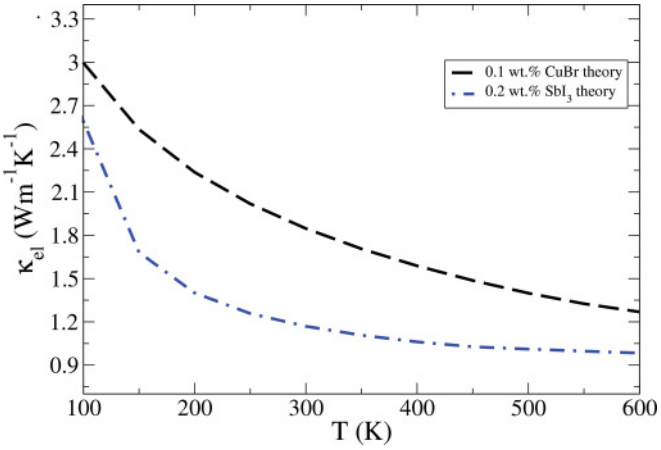

FIG. 4. (Color online) Theoretical calculation of electronic thermal conductivity as a function of temperature for $Bi_2(Te_{0.85}Se_{0.15})_3$ single crystal doped with 0.1 wt % CuBr (dashed curve) and 0.2 wt % SbI_3 (dash-dotted curve).

and 1.26 $Wm^{-1}K^{-1}$ at 600 K for CuBr-doped samples and 2.58 $Wm^{-1}K^{-1}$ at 100 K and 0.98 $Wm^{-1}K^{-1}$ at 600 K for SbI_3-doped samples. It is interesting to note that we did not find any significant difference in the results whether the samples were regarded as extrinsic only or with the consideration of the extrinsic-intrinsic turnover.

2. *Bipolar thermal conductivity*

The theoretical calculation of bipolar thermal conductivities of both samples are presented in Fig. 5. This contribution is significant only at high temperatures (typically above 150 K). According to Eq. (17) it increases at least linearly with temperature. For temperature change from 200 to 600 K the rise in κ_{bp} is 1.95 $Wm^{-1}K^{-1}$ for SbI_3-doped samples and 1.54 $Wm^{-1}K^{-1}$ for CuBr-doped samples, which we believe is mainly due to different energy band-gap variations with temperature.

Up to 300 K, the bipolar thermal conductivity is insignificant compared to the electronic thermal conductivity, and κ_{el}

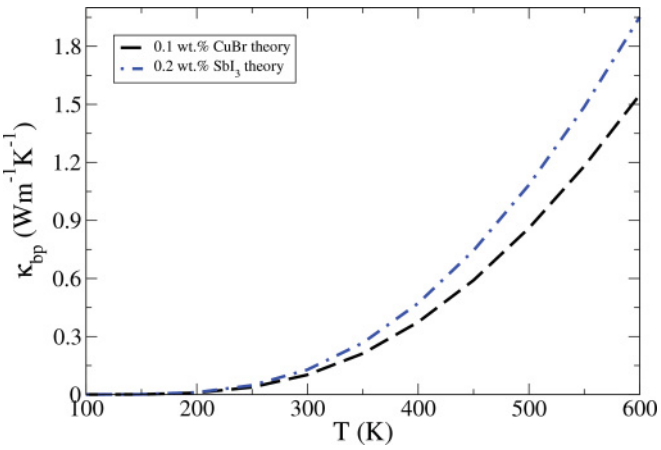

FIG. 5. (Color online) Theoretical calculation of bipolar thermal conductivity as a function of temperature for $Bi_2(Te_{0.85}Se_{0.15})_3$ single crystal doped with 0.1 wt % CuBr (dashed curve) and 0.2 wt % SbI_3 (dash-dotted curve).

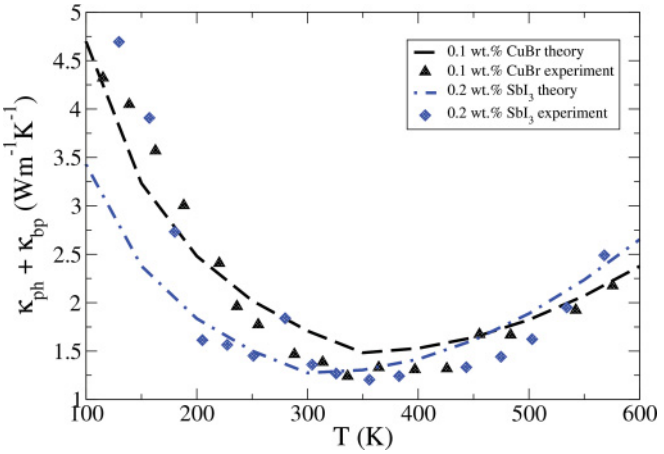

FIG. 6. (Color online) Sum of lattice and bipolar contributions of thermal conductivities for $Bi_2(Te_{0.85}Se_{0.15})_3$ single crystal doped with 0.1 wt % CuBr (dashed curve) and 0.2 wt % SbI_3 (dash-dotted curve). The symbols represent the extracted values of $\kappa_{total} - \kappa_{el}$ by Hyun *et al.*[19]

is lower for SbI_3-doped samples. At 600 K, on the other hand, κ_{bp} is larger than κ_{el}, but the sum $\kappa_{bp} + \kappa_{el}$ is nearly the same for both samples.

3. *Phonon thermal conductivity*

The lattice (phonon) plus bipolar thermal conductivity results are shown in Fig. 6 and compared with the $\kappa_{total} - \kappa_{el}$ values from Hyun *et al.*[19] We point out that the present calculations for κ_{ph} involve the use of a single semiadjustable parameter $F_{3ph} = (\frac{\gamma}{c})^2$.

For both samples, at low temperatures (below 100 K) boundary and electron-phonon scatterings are dominant. Mass defect scatterings (with the source of isotopic and alloy effects) are important at both low and high temperatures. Phonon-phonon interactions become particularly important at high temperatures (above 100 K) for both materials. Although not shown in a separate graph, in the high-temperature regime (i.e., above the Debye temperature of 155 K for bulk Bi_2Te_3) the phonon conductivity decreases linearly with temperature.

4. *Frequency dependence of phonon thermal conductivity*

In Fig. 7 we present the spectral analysis of the conductivity in frequency space for the 0.2 wt % SbI_3-doped $Bi_2(Te_{0.85}Se_{0.15})_3$ single crystal at several temperatures. We make a few important observations. At low temperatures, most heat is conducted by phonons of low frequencies. At high temperatures, phonons over a very large frequency range provide significant contribution to the conductivity. For example, at 50 and 500 K, up to 80% contribution comes from phonons in the frequency range $1.9 \leqslant \omega \leqslant 13.6$ THz, and $6.4 \leqslant \omega \leqslant 17.8$ THz, respectively. The peak of the κ-ω spectrum shifts to the higher values of frequency with increase in temperature. This is consistent with the theoretical result presented by Garg *et al.*[33] for the study of the phonon conductivity in a SiGe alloy. In the present study we also find that while the spectrum peaks at the frequency $\omega_D/3$ at 50 K (where ω_D is the Debye frequency), it becomes $\omega_D/1.25$ at around 600 K. The shift in the peak of the κ-ω spectrum toward

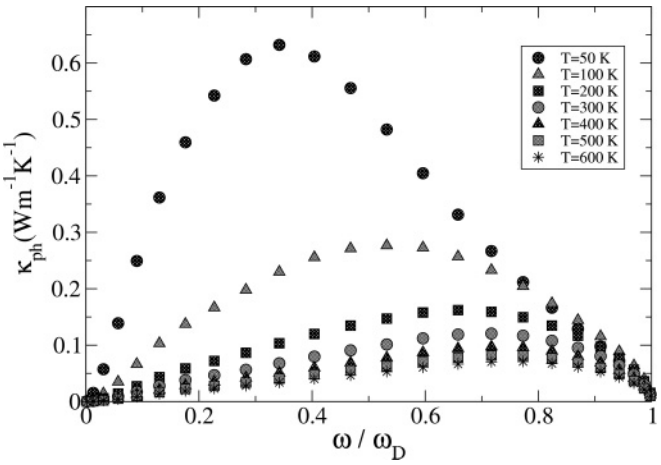

FIG. 7. Frequency dependence of phonon thermal conductivity for different temperatures for 0.2 wt % SbI_3-doped $Bi_2(Te_{0.85}Se_{0.15})_3$ single crystal where the Debye frequency is taken as $\omega_D = 18.92$ THz.

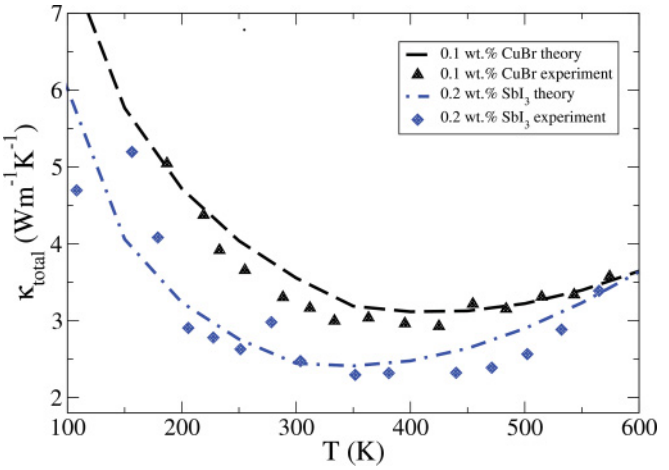

FIG. 8. (Color online) Temperature variation of total thermal conductivity for $Bi_2(Te_{0.85}Se_{0.15})_3$ single crystal doped with 0.1 wt % CuBr (dashed curve) and 0.2 wt % SbI_3 (dash-dotted curve). The symbols represent the experimental results from Ref. 19.

higher frequency with increase in temperature is consistent with the concept of dominant phonon approximation, which following the prescription by Ziman[34] can be defined as $\hbar\omega_{\rm dom} \simeq 1.6k_BT$.

Recently, Koh and Cahill[35] studied the frequency dependence of the lattice thermal conductivity of semiconductor alloys by employing the time-domain thermoreflectance technique over a low-frequency range and a reasonably large temperature range. Such measurements are considered to provide a convenient method for probing the phonon distribution of materials. Their results clearly show that $\kappa(\lambda)$ increases with decrease in the mean free path λ. Noting the general relationship between the phonon mean free path and frequency as $\lambda \propto \omega^{-n}$,[34] our results presented in Fig. 7, in the frequency range from zero up to the maximum in the $\kappa(\omega)$ spectrum at any temperature, provide support for the measurements made by Koh and Cahill.

5. *Total thermal conductivity*

As seen in Fig. 8, there is an overall good agreement between our results for the total thermal conductivity and the experimental data presented by Hyun *et al.*[19] As stated earlier, in the high-temperature range the phonon conductivity decreases linearly and the bipolar contribution rises at least linearly with temperature. Thus, the sum of the phonon and bipolar thermal conductivity contributions, $\kappa_{\rm ph} + \kappa_{\rm bp}$, shows a dip at around 350 K for both samples. The experimental measurements by Hyun *et al.* suggest that there is a switchover in the temperature variation of $\kappa_{\rm ph} + \kappa_{\rm bp}$ for the two alloys at around 450 K: the sum of these two contributions is lower for the SbI_3-doped sample below 450 K and for the CuBr-doped sample above 450 K. We successfully reproduced this switchover with the choice of parameters listed in Table I.

C. Figure of merit

The thermoelectric efficiencies of both 0.1 wt % CuBr- and 0.2 wt % SbI_3-doped $Bi_2(Te_{0.85}Se_{0.15})_3$ single crystals are reported in Fig. 9. There is a reasonably good level of agreement between our theoretical results, obtained by considering both extrinsic and intrinsic characteristics of the two samples, and the experimental measurements by Hyun *et al.*[19] Calculations based on only extrinsic consideration produce worse agreement with experimental data at the higher-temperature end, with more disagreement for the SbI_3-doped sample. These disagreements originate from the disagreements noted earlier for the Seebeck coefficient.

In the extrinsic regime the SbI_3-doped alloy sample has only a slightly larger efficiency than the CuBr-doped sample. This is because both the ratio of the power factor ($S^2\sigma$) and the $\kappa_{\rm total}$ between the samples are nearly equal to each other. At high temperatures (in the intrinsic regime) the CuBr-doped alloy sample has larger efficiency. This is due to the higher value of the power factor for the CuBr-doped sample.

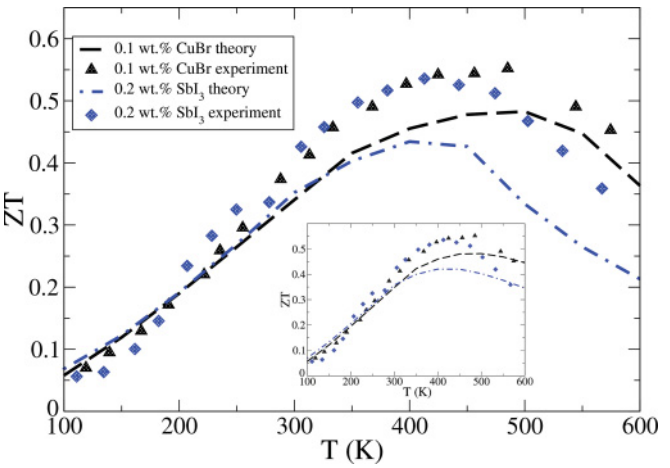

FIG. 9. (Color online) Temperature variation of figure of merit for $Bi_2(Te_{0.85}Se_{0.15})_3$ single crystal doped with 0.1 wt % CuBr (dashed curve) and 0.2 wt % SbI_3 (dash-dotted curve). The symbols are experimentally expected values from the work by Hyun *et al.*[19] The inset shows the results of treating the samples as extrinsically doped throughout the entire temperature range.

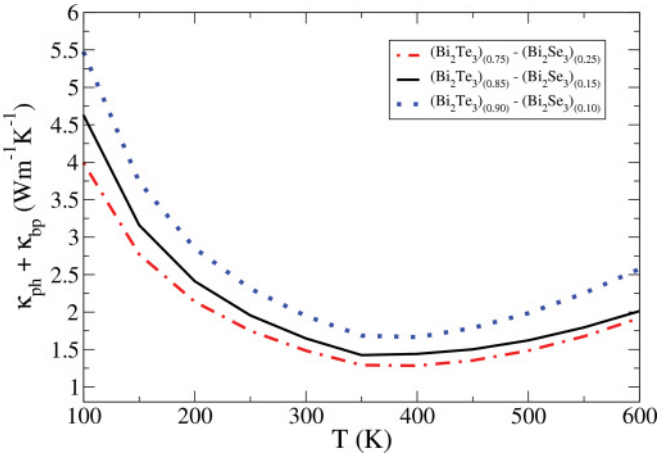

FIG. 10. (Color online) Theoretical calculation of the sum of lattice and bipolar contributions of thermal conductivities for $(Bi_2Te_3)_x(Bi_2Se_3)_{(1-x)}$ alloys, taking the value of x as 0.75, 0.85, and 0.90.

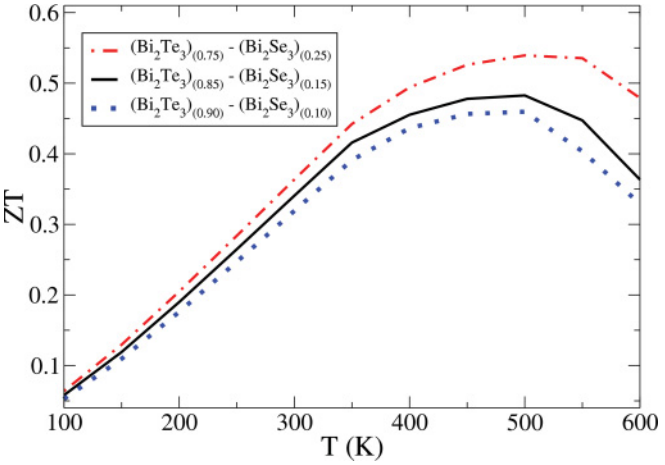

FIG. 11. (Color online) Theoretical calculation of thermoelectric figure of merit for $(Bi_2Te_3)_x(Bi_2Se_3)_{(1-x)}$ alloys, taking the value of x as 0.75, 0.85, and 0.90.

D. Effect of alloying on figure of merit

As stated earlier, phonon-alloy scattering results in lowering of thermal conductivity and enhancement in thermoelectric efficiency. To investigate the effect of alloying on the 0.1 wt % CuBr-doped sample, we used different amounts of Te/Se content in the $(Bi_2Te_3)_x(Bi_2Se_3)_{(1-x)}$ single crystal. The parameters to calculate $\kappa_{ph} + \kappa_{bp}$ for $x = 0.75$ and $x = 0.90$ are taken as $E_g(0) = (0.24,0.20)$ eV, $q_D = (0.715,0.71)$ Å^{-1}, lattice constant $a_{lat} = (4.321,4.358)$ Å, $\rho = (7.67,7.7)$ g/cm^3, and $\Omega = (162.2,166.3)$ Å^3, respectively. The parameters for $x = 0.85$ have already been given in Table I. The temperature dependence of $\kappa_{ph} + \kappa_{bp}$ for all three different x values is presented in Fig. 10. It is clearly seen that by decreasing the x value (i.e., by increasing Se content) the thermal conductivity becomes lower throughout the entire temperature range due to the increase in the alloy scattering. We predict that by decreasing the x value from 0.90 to 0.75 (i.e., increasing the Se concentration from 10% to 25%) the reduction in $\kappa_{ph} + \kappa_{bp}$ would be 40% at 200 K and 44.5% at 600 K. Consistent with this variation, ZT would be enhanced by 33% and 50% at 200 and 600 K, respectively (Fig. 11).

E. Effect of full-scale thermal conductivity calculation on ZT

As discussed earlier, κ_{ph} is the most important parameter to obtain higher values of ZT. Thus, correctly defining and calculating the lattice thermal conductivity of a material has a crucial importance in discussing thermoelectricity. We elaborate on this point by considering two examples. In the first example we consider the work of Vining,[14] who considered the anharmonic phonon scattering as $\tau_{anh}^{-1} \propto C\omega^2 T$, where C is a constant of temperature. We note that this assumption is only true in the high-temperature regime.[16] Vining further considered a single, polarization-average phonon branch, expressed as $\tau_N^{-1}/\tau_U^{-1} = \beta$, and treated β as a constant of temperature. To make a comparison between our theoretical approach and the Vining model,[14] we made a calculation for the temperature dependence of $\kappa_{ph} + \kappa_{bp}$ for the $Bi_2(Te_{0.85}Se_{0.15})_3$ single crystal doped with 0.1 wt % CuBr. For employing Vining's approach, we fitted the parameter $C = 3.25 \times 10^{-7}$ s^3/K from our theoretical κ_{ph} value at 600 K (the highest temperature in our study). Then with this fixed value of C and $\beta = 2.0$, we calculated κ_{ph} and added the temperature dependence of the bipolar thermal conductivity for the whole temperature range. As clearly seen in Fig. 12, Vining's approach cannot explain the experimental results at low temperatures. For example, at 110 K Vining's approach gives $\kappa_{ph} + \kappa_{bp} = 2.1$ Wm^{-1}K^{-1}, while the experimental result as well as our theoretical result are close to 4.3 Wm^{-1}K^{-1}.

From our model we find the following values of β_{LA}, β_{TA}: 1.8, 0.17 at 100 K and 1.65, 0.18 at 600 K. Thus, while β is rather temperature insensitive for transverse acoustic (TA) modes, it does increase with decrease with temperature for longitudinal acoustic (LA) modes. Our estimate of the temperature-average (over the range considered in our study) value of β is 1.7 for LA modes, 0.18 for TA modes, and 0.7 for polarization-averaged modes. We thus find that Vining's choice of β is only reasonable for LA phonons.

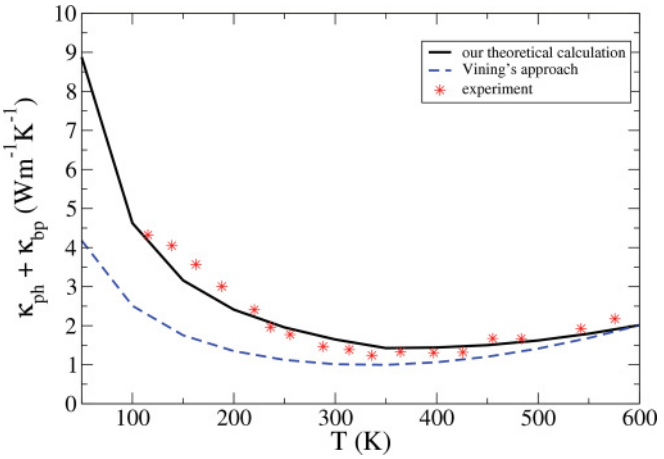

FIG. 12. (Color online) Comparison of $\kappa_{ph} + \kappa_{bp}$ calculation between our theoretical model and Vining's approach[14] for a $Bi_2(Te_{0.85}Se_{0.15})_3$ single crystal doped with 0.1 wt % CuBr.

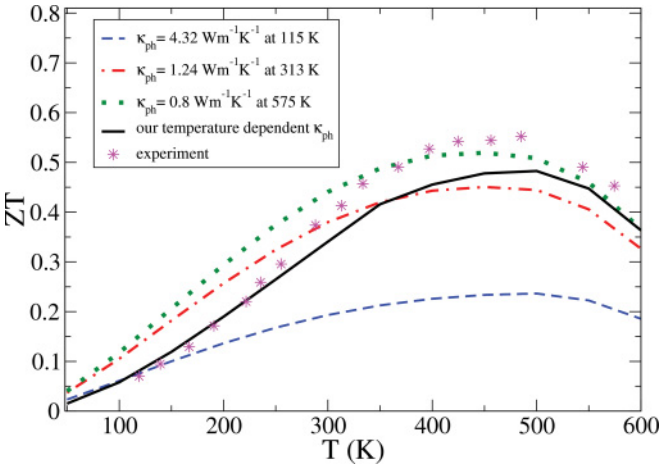

FIG. 13. (Color online) Comparison of ZT calculation between our theoretical model and Hicks and Dresselhaus' approach[15] for a $Bi_2(Te_{0.85}Se_{0.15})_3$ single crystal doped with 0.1 wt % CuBr.

As a second example, we consider the work of Hicks and Dresselhaus,[15] who treated κ_{ph} as a constant (temperature independent). As shown in Fig. 13, to test this approach, we took three different κ_{ph} values at 115, 313, and 575 K by subtracting the theoretical values of κ_{bp} from the experimental measurements of $\kappa_{total} - \kappa_{el}$ reported by Hyun *et al.*[19] With any one of these three choices we are unable to fit the experimentally determined magnitude and temperature dependence of ZT at low temperatures (below 300 K). At high temperatures (above 300 K), due to the dominant behavior of the bipolar contribution of thermal conductivity in this temperature regime, the magnitude of ZT comes closer to our theoretical model by taking the values of κ_{ph} at 313 and 575 K.

From the above two examples, we can conclude that in order to obtain the correct magnitude and temperature variation of ZT it is important to include the correct magnitude and temperature dependence of κ_{ph} in both low- and high-temperature regimes. Our model of phonon conductivity is helpful in this respect.

IV. SUMMARY AND OUTLOOK

We have studied the thermoelectric properties of the n-type $Bi_2(Te_{0.85}Se_{0.15})_3$ single crystal, containing 0.1 wt % CuBr and 0.2 wt % SbI_3 dopants, by considering all the transport coefficients systematically and fully. The present theoretical and computational procedure for the evaluation of the lattice thermal conductivity is much more rigorous than attempted before.

The temperature variation of the Fermi energy reveals that the CuBr-doped sample, with dopant concentration of 1.32×10^{25} m^{-3}, is extrinsic up to 500 K and becomes intrinsic beyond that temperature. The SbI_3-doped sample, with a lower dopant concentration of 8.0×10^{24} m^{-3}, ceases to be extrinsic beyond 450 K. With these features of the Fermi energy, the Seebeck coefficient has almost similar magnitude for both samples up 450 K, but decreases more sharply for the SbI_3-doped sample beyond that temperature. Both the electrical conductivity and the electronic thermal conductivity of the CuBr-doped sample are found to be higher throughout the temperature range 100–600 K considered in this work. The electron-hole bipolar contribution to the thermal conductivity is similar for the two samples up to 300 K, beyond which it is found to be lower for the CuBr-doped sample.

The total thermal conductivity (sum of electronic, bipolar, and lattice contributions) is higher for the CuBr-doped sample throughout the temperature range of our investigations. An analysis of the frequency spectrum of the thermal conductivity suggests that while at low temperatures most heat is conducted by phonons of low frequencies, at high temperatures phonons over a very large frequency range provide a significant contribution to the conductivity. The peak of the $\kappa(\omega)$ spectrum shifts to higher frequencies as temperature increases.

The magnitude and temperature variation of the figure of merit, ZT, is similar for both samples up to 400 K, and decreases faster for the SbI_3-doped sample beyond that temperature. The calculated maximum value of ZT is 0.43 and 0.49 for the SbI_3- and CuBr-doped samples, respectively. Our results for each of the thermoelectric transport coefficients (S, σ, κ) and ZT are in reasonable agreement with the experimental measurements reported by Hyun *et al.*[19]

The effect of alloying on thermoelectric efficiency is investigated. It is found that due to the reduction in phonon thermal conductivity, a reasonable increase in the Se content in $(Bi_2Te_3)_x(Bi_2Se_3)_{(1-x)}$ single crystals can increase ZT significantly at both low and high temperatures.

The present systematic approach for explaining the thermoelectric properties of three-dimensional semiconductor structures will be extended to low-dimensional structures in the future.

ACKNOWLEDGMENTS

Övgü Ceyda Yelgel is grateful for financial support from the Republic of Turkey Ministry of National Education through the University of Rize in Turkey (Rize Üniversitesi Rektörlüğü, Fener Mah. Merkez Kampüs 53100/RİZE/TÜRKİYE).

[1] J.-C. Zheng, Front. Phys. China **3**, 269 (2008).
[2] C. Wood, Energy Convers. Manage. **24**, 317 (1984).
[3] D. M. Rowe, Int. Journal of Innovations in Energy Systems and Power **1**, 13 (2006).
[4] Y. Lan, A. J. Minnich, G. Chen, and Z. Ren, Adv. Funct. Mater. **20**, 357 (2010).
[5] T. M. Tritt, *Recent Trends in Thermoelectric Materials Research I* (Academic Press, San Diego, 2001).
[6] D. M. Rowe, *Thermoelectrics Handbook* (Taylor & Francis, London, 2006).
[7] R. R. Heikes and R. W. Ure, *Thermoelectricity, Science and Engineering* (Interscience, New York, 1961).
[8] A. F. Ioffe, *Semiconductor Thermoelements and Thermoelectric Cooling* (Infosearch, London, 1957).
[9] B. Poudel, Q. Hao, Y. Ma, Y. Lan, A. Minnich, B. Yu, X. Yan, D. Wang, A. Muto, D. Vashaee, X. Chen, J. Liu, M. S. Dresselhaus, G. Chen, and Z. Ren, Science **320**, 634 (2008).
[10] R. Venkatasubramanian, E. Siivola, T. Colpitts, and B. O'Quinn, Nature (London) **413**, 597 (2001).

[11] V. Goyal, D. Teweldebrhan, and A. A. Balandin, Appl. Phys. Lett. **97**, 133117 (2010).
[12] F. Zahid and R. Lake, Appl. Phys. Lett. **97**, 212102 (2010).
[13] H. J. Goldsmid, *Introduction to Thermoelectricity* (Springer-Verlag, Berlin, 2010).
[14] C. B. Vining, J. Appl. Phys. **69**, 331 (1991).
[15] L. D. Hicks and M. S. Dresselhaus, Phys. Rev. B **47**, 12727 (1993).
[16] G. P. Srivastava, *The Physics of Phonons* (Taylor & Francis, New York, 1990).
[17] P. J. Price, Phil. Mag. **46**, 1252 (1955).
[18] J. P. McKelvey, *Solid State and Semiconductor Physics* (Harper & Row, New York, 1966).
[19] D. B. Hyun, J. S. Hwang, B. C. You, T. S. Oh, and C. W. Hwang, J. Mater. Sci. **33**, 5595 (1998).
[20] D. M. Rowe and C. M. Bhandari, *Modern Thermoelectrics* (Reston Publishing, Reston, VA, 1983).
[21] B. R. Nag, *Theory of Electrical Transport in Semiconductors* (Pergamon, Oxford, 1972).
[22] R. R. Heikes and R. W. Ure, *Thermoelectricity: Science and Engineering* (Interscience, New York, 1961).
[23] T. M. Tritt, *Thermal Conductivity Theory, Properties and Applications* (Kluwer Academic/Plenum, London, 2004).
[24] A. H. Wilson, *The Theory of Metals* (Cambridge University Press, London, 1953).
[25] C. J. Glassbrenner and G. A. Slack, Phys. Rev. **134**, A1058 (1964).
[26] M. G. Holland, Phys. Rev. **134**, A471 (1964).
[27] J. E. Parrott, Rev. Int. Hautes Temp. Refract. **16**, 393 (1979).
[28] D. R. Lide, *CRC Handbook of Chemistry and Physics*, 87th ed. (Taylor & Francis, London, 2007).
[29] L. W. Silva and M. Kaviany, Int. J. Heat Mass Transfer **47**, 2417 (2004).
[30] W. Zhang, R. Yu, H. Zhang, X. Dai, and Z. Fang, New J. Phys. **12**, 065013 (2010).
[31] J. S. Blakemore, *Solid State Physics* (Saunders, London, 1970).
[32] C. Kittel, *Introduction to Solid State Physics*, 8th ed. (Wiley, New York, 2005).
[33] J. Garg, N. Bonini, B. Kozinsky, and N. Marzari, Phys. Rev. Lett. **106**, 045901 (2011).
[34] J. M. Ziman, *Electrons and Phonons* (Clarendon, Oxford, 1960).
[35] Y. K. Koh and D. G. Cahill, Phys. Rev. B **76**, 075207 (2007).